

Quantum capacitance in monolayers of silicene and related buckled materials

S. Nawaz[†] and M. Tahir^{*}

[†]*CNR-IOM Laboratorio TASC, Area Science Park, Basovizza, 34149 Trieste, Italy and International Centre for Theoretical Physics (ICTP),*

I-34014 Trieste, Italy, and CDL, Physics Division, PINSTECH, P. O. Nilore, Islamabad, Pakistan and

**Department of Physics, Concordia University, Montreal, Quebec, Canada H3G 1M8*

Abstract

Silicene and related buckled materials are distinct from both the conventional two dimensional electron gas and the famous graphene due to strong spin orbit coupling and the buckled structure. These materials have potential to overcome limitations encountered for graphene, in particular the zero band gap and weak spin orbit coupling. We present a theoretical realization of quantum capacitance which has advantages over the scattering problems of traditional transport measurements. We derive and discuss quantum capacitance as a function of the Fermi energy and temperature taking into account electron-hole puddles through a Gaussian broadening distribution. Our predicted results are very exciting and pave the way for future spintronic and valleytronic devices.

I. INTRODUCTION

It is now well established that graphene is the ever first stable material with two dimensional (2D) electronic structure. Graphene does not only carry the exceptional electronic properties but also has enormous potential for applications in various fields [1]. However, its applications to electronic industry are challenging due to the absence of an intrinsic band gap and very weak spin-orbit coupling (SOC). Therefore, a race has begun in search of other similar materials which could over rule the limiting factors of graphene. Indeed, the first choice to explore was to study the close relatives of carbon i.e., silicon, germanium and tin for the stability of their 2D sheets [2]. The motivation begins due to the existence of an intrinsic energy gap in these materials and to their larger ionic radii. Nevertheless the later lead to their 2D buckled honeycomb lattice structures with enhanced SOC.

In recent years, there is a lot of experimental progress towards the realization of stable silicene [3, 4]. Silicene is an excellent material for electronic applications due to its compatibility with the existing Si-based technology. Moreover, the realization of stable 2D structures of silicene, germanene and stanene provides an exciting state of matter beyond graphene. These layered materials open the possibility to explore 2D systems with strong SOC and structural buckling. Additionally, the band gap of silicene is tunable by an external perpendicular electric field applied along the buckling direction [5, 6]. In the meanwhile, theoretical studies have predicted the stability of silicene on different substrates such as graphene [7, 8], boron nitride, silicon carbide [9] and solid argon [10]. Recently, silicene and germanene have been grown and realized to be stable at room temperature on gold and silver surfaces as well [11–13]. Nevertheless silicene field effect transistors (FETs) have been demonstrated most recently [14]. These materials are expected to show exotic properties such as quantum spin- and valley-Hall effects among many others [15–17]. Although the focus of silicene research has been towards its transport properties, however, insight into its fundamental electronic properties and device physics still calls for knowledge about the capacitance-voltage (C-V) characteristics.

Quantum capacitance can be effectively used to probe the thermodynamical density of states (DOS). These measurements not only provide an important way to understand the fundamental electronic properties of materials but also have potential utilization in device fabrication. For instance, the study of quantum capacitance in graphene has shown impor-

tant implications on the design of FETs [18–23]. Moreover, the quantum capacitance has advantages over traditional transport measurements whereas the latter are more complicated and sensitive to scattering details. Furthermore, to improve the performance of FETs, the potential of silicene as a channel material is creating much excitement due to strong SOC and tunable buckled structures. This is because of its excellent intrinsic transport features as well as the possibility of patterning device structures within top-down lithographical approach. The present work aims at determining the combined effects of SOC and perpendicular electric field on quantum capacitance of silicene and related buckled materials. Quantum capacitance is described by $C_Q = e^2 D(E)$, where $D(E)$ represents the DOS, thus providing a quantitative description of the DOS at the Fermi energy. Despite its capability of directly probing electronic properties at finite temperatures, to the best of our knowledge, C_Q has not been studied for silicene, germanene and stanene.

II. MODEL FORMULATION

We consider a monolayer silicene by an effective Hamiltonian in xy-plane. An external perpendicular electric field is applied to the silicene sheet taking into account the effects of SOC. Dirac fermions in buckled silicene obey the 2D graphene-like Hamiltonian [2, 5, 6]

$$H_s^\eta = v(\eta\sigma_x p_x + \sigma_y p_y) + \eta s \lambda \sigma_z + \Delta \sigma_z \quad (1)$$

Here $\eta = +/−$ for K/K' valleys, $\Delta = 2lE_z$, where E_z is the uniform electric field with $l = 0.23 \text{ \AA}$. In addition, $(\sigma_x, \sigma_y, \sigma_z)$ is the vector of Pauli matrices, λ is SOC energy and v denotes the Fermi velocity of the Dirac fermions. The SOC energy for silicene, stanene and germanene is 3.9 meV, 29 meV and 43 meV, respectively [2]. The up and down spin states are represented by $s = +1$ and -1 , respectively. After diagonalizing the Hamiltonian given in Eq. (1), we obtain the energy eigenvalues

$$E_s^\eta = \pm \sqrt{v^2 \hbar^2 k^2 + (\Delta + \eta s \lambda)^2} \quad (2)$$

We employ the delta function to represent DOS as

$$D(E) = \sum_{\eta, s} \delta(E - E_s^\eta), \quad (3)$$

The evaluation of DOS is straightforward and yields us

$$D(E) = \sum_{\eta,s} \frac{g_s g_v |E|}{2\pi(\hbar v)^2} \theta[y]. \quad (4)$$

Here $\theta[y] \equiv \theta[|E| - |\Delta + \eta s \lambda|]$ is the Heaviside step function, g_s and g_v are spin and valley degeneracy factors, respectively. In the limits of zero SOC and electric field energies, the DOS reduces to standard graphene expression [19].

Further, it has been demonstrated that graphene exhibits inhomogeneous landscapes of electron-hole puddles around the Dirac point [24–28]. Puddles are more probable to occur in gapless graphene as compared to a fully gapped silicene. However, the possible existence of puddles and their effects in silicene layers are unexplored yet and needs to be addressed.

We start by assuming that charged impurities, located in the substrate or near the silicene surface, create a local electrostatic potential V which fluctuates randomly about its average value. The potential fluctuations are described by a statistical distribution function $P(V)$ where $V = V(r)$ is the fluctuating potential energy at the point $r \equiv (x, y)$ in the 2D silicene plane. The probability $P(V)dV$ of finding the local electronic potential energy within a range dV about V to a Gaussian form is approximated as [29, 33, 34]

$$P(V) = \frac{1}{\sqrt{2\pi}\Gamma} \exp\left[-\frac{V^2}{2\Gamma^2}\right] \quad (5)$$

Here Γ is the standard deviation (or equivalently, the strength of the potential fluctuation), which is used as an adjustable parameter to tune the Gaussian broadening [29].

The potential fluctuations given by Eq. (5) affect the overall electronic DOS. In our model we do not assume the size of the puddles to be identical, instead we take the puddle size to be completely random, controlled by the distribution function. We emphasize that our model provides an excellent quantitative approximation for the actual numerical calculations of puddle structures in graphene [30]. The characteristics of the puddles are determined by both the sign and the magnitude of $V - E_F$, i.e., a negative (positive) $V - E_F$ indicates an electron (hole) region. A different approach utilizing equal size puddles with a certain potential V has been implemented to calculate transport coefficients using a numerical transfer-matrix technique [30–32]. In the presence of electron-hole puddles the C_Q is given by

$$C_Q = \frac{e^2}{\sqrt{2\pi}\Gamma} \int_{-\infty}^E D(E) \exp\left[-\frac{V^2}{2\Gamma^2}\right] dV \quad (6)$$

Using Eq. (4) into Eq. (6) the C_Q is simplified to

$$C_Q = \frac{e^2 D_1}{\sqrt{2\pi}\Gamma} \left[\int_{-\infty}^E \sqrt{2}\Gamma E \exp(-x^2) dx + \int_{-\infty}^E (\sqrt{2}\Gamma)^2 x \exp(-x^2) dx \right] \theta[y] \quad (7)$$

Here $D_1 = \frac{g_s g_v}{2\pi(\hbar v)^2}$ and $x = \frac{V}{\sqrt{2}\Gamma}$. Using the definition of error function ($\sqrt{\pi}[1 + \text{erf}(x)]/2 = \int_{-\infty}^x \exp[-(x')^2] dx'$), we arrive at the final result

$$C_Q = e^2 \sum_{\eta,s} D_1 \left[\frac{E}{2} \text{erfc}\left[-\frac{E}{\sqrt{2}\Gamma}\right] + \frac{\Gamma}{\sqrt{2\pi}} \exp\left(-\frac{E^2}{2\Gamma^2}\right) \right] \theta[y] \quad (8)$$

where $\text{erfc}(x)$ is the complementary error function. Due to the electron-hole symmetry in the problem, we only provide the formalism and equations for electron like carriers and the hole part can be obtained simply by changing E to $-E$. For the case $\Gamma = 0$, the system becomes homogeneous and $C_Q = e^2 D_1 E \theta[y]$, which is similar to that obtained in Eq. (4). In this case there is no carrier density at the Dirac point ($E = 0$) at zero temperature. Further, it is apparent that in the presence of potential fluctuations, the C_Q starts at finite value at $E = 0$ and approaches $e^2 D_1 E \theta[y]$ in the limits of high-energy and finite Γ . For the high-energy limits, the carriers are essentially free. The electron density at finite temperatures increases due to thermal excitations from valence band to conduction band, which is one of the important sources of temperature-dependent transport at low carrier densities.

Eq. (8) shows dependence of C_Q upon Fermi energy along with SOC and electric field energies. However, by taking into account the effects of low energy excitations like charge impurities or puddles, C_Q is plotted in Fig. 1 as a function of Fermi energy. It is evident from the results that the system carries two energy gaps around the Dirac point (solid lines) due

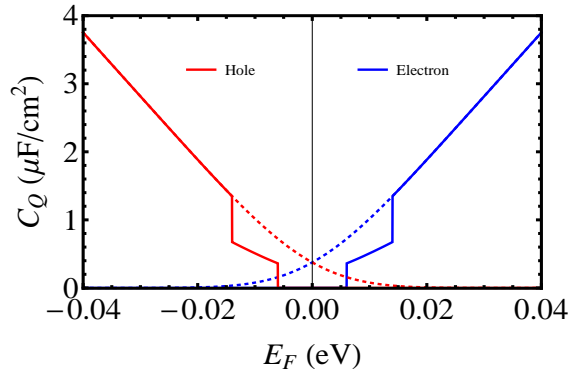


FIG. 1. Quantum capacitance as a function of the Fermi energy for $\Gamma = 10$ meV and $T = 0K$. The dotted and solid curves correspond to $\Delta = \lambda = 0$ and $\Delta = 10$ meV with $\lambda = 4$ meV, respectively.

to the presence of both the applied electric field and strong SOC energies. These gaps are tunable by varying the perpendicular electric field. One may notice that there is negligible puddle effect in silicene (solid line). In contrast, Eq. (8) reduces to gapless spectrum of graphene when the applied field and SOC energies are switched to zero (dotted lines) and hence we can see the puddle effect.

To observe the expected puddle effect in silicene in detail, we show C_Q as a function of the Fermi energy in Fig. 2. We find that the potential fluctuations caused by puddles in graphene affect the C_Q considerably around the Dirac point (left panel). Contrary to this, the same effect seems significantly suppressed in silicene as shown in Fig. 2 (right panel). Further, it is interesting to note that the electric field will lead to tuning of the C_Q in the presence of puddles.

In silicene and related buckled materials there is an extensive interest towards the realization of quantum phase transitions [5, 6, 15–17]. In these materials, the transitions are driven by tuning the perpendicular electric field in different regimes. In Fig. 3, we show quantum phase transitions for monolayer silicene as a function of the Fermi energy. The dotted curve corresponds to topological insulating state, where $\lambda = 4$ meV and $\Delta = 0$ meV. Here the width of the Gaussian broadening is fixed to 10 meV. The semi-metallic state for $\lambda = \Delta = 4$ meV is shown in dot-dashed curve. The solid curve represents the band insulating state, where $\lambda = 4$ meV and $\Delta = 20$ meV. We believe that these transitions would be easy to probe through the measurements of DOS and the corresponding C_Q . This is because the

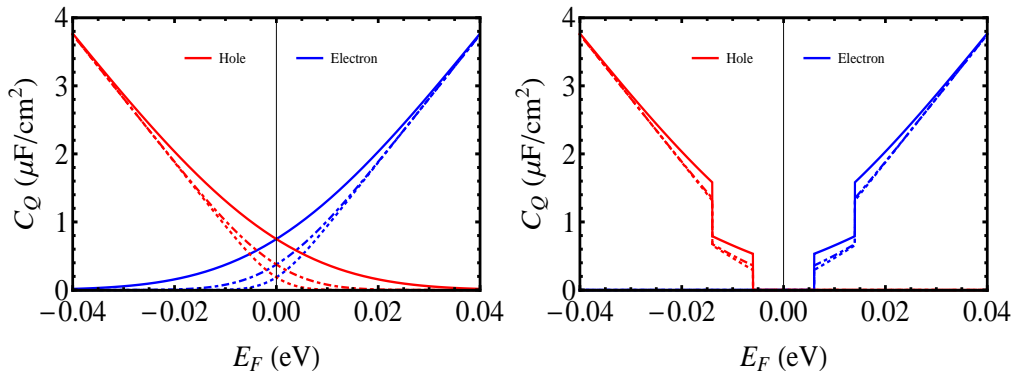


FIG. 2. Quantum capacitance as a function of the Fermi energy for $T = 0K$, $\Gamma = 5$ meV (dotted curves), $\Gamma = 10$ meV (dot-dashed curves), and $\Gamma = 20$ meV (solid curves). The right panel is for $\Delta = \lambda = 0$ and the left panel for $\Delta = 10$ meV and $\lambda = 4$ meV.

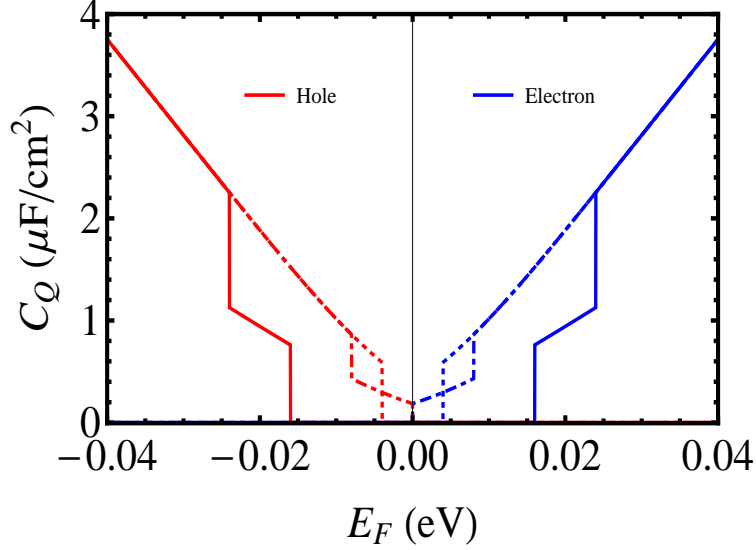


FIG. 3. Quantum capacitance as a function of the Fermi energy for $T = 0K$, $\Gamma = 10$ meV and $\lambda = 4$ meV. The dotted, dot-dashed, and solid curves correspond to $\Delta = 0$ meV, $\Delta = 4$ meV, and $\Delta = 20$ meV, respectively.

C_Q has advantages over scattering complications in traditional transport measurements.

Next we discuss the effects of temperature on C_Q of the system under consideration. The C_Q is defined as the derivative of the total net charge of the system with respect to applied electrostatic potential [19]. The total charge is proportional to the weighted average of C_Q at the Fermi level E_F . When the DOS as a function of energy is known, the C_Q at finite temperature can be written as

$$C_Q = e^2 \int_{-\infty}^{+\infty} D(E) \left(-\frac{\partial f(E - E_F)}{\partial E} \right) dE \quad (9)$$

One should note that the above expression is clearly valid for any temperature and Fermi energy. Here we show temperature dependent C_Q in Fig. 4 as a function of the Fermi energy. We evaluate numerically C_Q using Eq. (9) for a fixed value of Gaussian broadening $\Gamma = 1$ meV. The blue and red solid curves correspond to $T = 5K$ and $30K$, respectively. We note that by increasing the temperature, the effects of SOC and electric field are washed out. In contrast, black dotted curve represents graphene in the limits of $\lambda = \Delta = 0$ for a fixed temperature of $5K$. To observe these transitions, the broadening of the levels must be less than the SOC and electric field energies. A similar value of the level broadening has been already achieved in high mobility graphene samples [35].

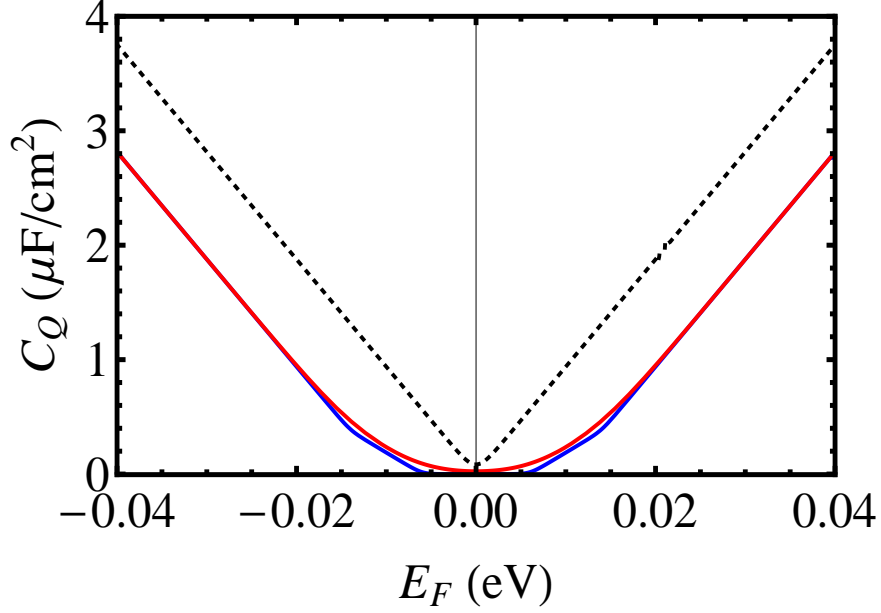


FIG. 4. Quantum capacitance as a function of the Fermi energy for $\Gamma = 1$ meV. The dotted and solid curves correspond to $\Delta = \lambda = 0$ and $\Delta = 10$ meV with $\lambda = 4$ meV, respectively. The dotted black and solid blue curves are for 5 K and solid red curve corresponds to 30 K.

The Hamiltonian in Eq. (1) can also be used to describe germanene and stanene, which are honeycomb structures similar to silicene. In these materials, the SOC energy is even stronger i.e. 43 meV (germanene) and 29 meV (stanene) [2]. Hence, the above analysis is fully applicable to the systems like germanene and stanene as well. Our results imply that the level splitting can be controlled by varying an external perpendicular electric field. We believe that the predicted analysis is very exciting and opens the possibility for future spintronic and valleytronic devices.

III. CONCLUSION

We have presented a theoretical model for the realization of quantum capacitance in monolayers of silicene and related buckled materials. For this, we employed the concept of broadened density of states taking into account electron-hole puddles through a Gaussian distribution. The quantum capacitance has two jumps around the Dirac point which are representative of two energy gaps. These gaps show significant signatures of quantum phase transitions as a competing consequence of SOC and electric field energies. Away from the

Dirac point, the quantum capacitance becomes linear as a function of Fermi energy. As temperature increases, two jumps around the Dirac point are washed out, while quantum capacitance remains nearly unchanged otherwise. In contrast to graphene, in the low temperature regime it seems that the effects of the electron-hole puddles are suppressed. We believe that these predictions open the possibility for tunable future spintronic and valleytronic devices based on silicene and related buckled materials.

Acknowledgments: S. N. would like to acknowledge the financial support by the ICTP and CNR-IOM Trieste, Italy.

Electronic addresses:

[†]shadi665@gmail.com, ^{*}m.tahir06@alumni.imperial.ac.uk,

-
- [1] C. Lee, Q. Li, W. Kalb, X.-Z. Liu, H. Berger, R. W. Carpick, and J. Hone, *Science* **328**, 76 (2010).
 - [2] C.-C. Liu, H. Jiang, and Y. Yao, *Phys. Rev. B* **84**, 195430 (2011).
 - [3] B. Lalmi, H. Oughaddou, H. Enriquez, A. Kara, S. Vizzini, B. Ealet, and B. Aufray, *Appl. Phys. Lett.* **97**, 223109 (2010); P. Vogt, P. D. Padova, C. Quaresima, J. Avila, E. Frantzeskakis, M. C. Asensio, A. Resta, B. Ealet, and G. L. Lay, *Phys. Rev. Lett.* **108**, 155501 (2012); A. Fleurence, R. Friedlein, T. Ozaki, H. Kawai, Y. Wang, and Y. Y. Takamura, *Phys. Rev. Lett.* **108**, 245501 (2012).
 - [4] C. L. Lin, R. Arafune, K. Kawahara, M. Kanno, N. Tukahara, E. Minamitani, Y. Kim, M. Kawai, and N. Takagi, *Phys. Rev. Lett.* **110**, 076801 (2013).
 - [5] N. D. Drummond, V. Zólyomi, and V. I. Fal’ko, *Phys. Rev. B* **85**, 075423 (2012).
 - [6] M. Ezawa, *New J. Phys.* **14**, 033003 (2012).
 - [7] Y. Cai, C.-P. Chuu, C. M. Wei, and M. Y. Chou, *Phys. Rev. B* **88**, 245408 (2013).
 - [8] M. N.-Amal, A. Sadeghi, G. R. Berdiyrov, and F. M. Peeters, *Appl. Phys. Lett.* **103**, 261904 (2013).
 - [9] H. Liu, J. Gao, and J. Zhao, *J. Phys. Chem. C*, **117**, 10353 (2013).

- [10] S. Sattar, R. Hoffmann, and U. Schwingenschlögl, *New J. Phys.* **16**, 065001 (2014).
- [11] M. E. Dávila, L. Xian, S. Cahangirov, A. Rubio, and G. Le. Lay, *New J. Phys.* **16**, 095002 (2014).
- [12] J. Sone, T. Yamagami, Y. Aoki, K. Nakatsuji, and H. Hirayama, *New J. Phys.* **16**, 095004 (2014).
- [13] P. D. Padova, C. Ottaviani, C. Quaresima, B. Olivieri, P. Imperatori, E. Salomon, T. Angot, L. Quagliano, C. Romano, A. Vona, M. M.-Miranda, A. Generosi, B. Paci, and G. L. Lay, *2D Materials* **1**, 021003 (2014).
- [14] L. Tao, E. Cinquanta, D. Chiappe, C. Grazianetti, M. Fanciulli, M. Dubey, A. Molle, and D. Akinwande, *Nature Nanotechnology* **10**, 227 (2015) .
- [15] M. Ezawa, *Phys. Rev. Lett.* **109**, 055502 (2012).
- [16] C. J. Tabert and E. J. Nicol, *Phys. Rev. B* **87**, 235426 (2013).
- [17] M. Tahir, A. Manchon, K. Sabeeh, and U. Schwingenschlögl, *Appl. Phys. Lett.* **102**, 162412 (2013).
- [18] S. Ilani, L. A. K. Donev, M. Kindermann, and P. L. McEuen, *Nat. Phys.* **2**, 687 (2006).
- [19] T. Fang, A. Konar, H. Xing, and D. Jena, *Appl. Phys. Lett.* **91**, 092109 (2007).
- [20] J. Guo, Y. Yoon, and Y. Ouyang, *Nano Lett.* **7**, 1935 (2007).
- [21] J. Xia, F. Chen, J. Li and N. Tao, *Nat. Nanotechnology* **4**, 505 (2009).
- [22] F. Giannazzo, S. Sonde, V. Raineri, and E. Rimini, *Nano Lett.* **9**, 23 (2009).
- [23] H. Xu, Z. Zhang, and L.-M. Peng, *Appl. Phys. Lett.* **98**, 133122 (2011).
- [24] J. Martin, N. Akerman, G. Ulbricht, T. Lohmann, J. H. Smet, K. v. Klitzing, and A. Yacoby, *Nat. Phys.* **4**, 144 (2008).
- [25] Y. Zhang, V. W. Brar, C. Girit, A. Zettl, and M. F. Crommie, *Nat. Phys.* **5**, 722 (2009).
- [26] A. Deshpande, W. Bao, F. Miao, C. N. Lau, and B. J. LeRoy, *Phys. Rev. B* **79**, 205411 (2009).
- [27] A. Deshpande, W. Bao, Z. Zhao, C. N. Lau, and B. J. LeRoy, *Phys. Rev. B* **83**, 155409 (2011).
- [28] E. Rossi and S. D. Sarma, *Phys. Rev. Lett.* **101**, 166803 (2008).
- [29] E. Arnold, *Appl. Phys. Lett.* **25**, 705 (1974).
- [30] P. S.-Jose, E. Prada, and D. S. Golubev, *Phys. Rev. B* **76**, 195445 (2007).
- [31] J. H. Bardarson, J. Tworzydło, P. W. Brouwer, and C. W. J. Beenakker, *Phys. Rev. Lett.* **99**, 106801 (2007).
- [32] E. Louis, J. A. Vergés, F. Guinea, and G. Chiappe, *Phys. Rev. B* **75**, 085440 (2007).

- [33] R. Zallen and H. Scher, Phys. Rev. B **4**, 4471 (1971).
- [34] T. P. Eggarter and M. H. Cohen, Phys. Rev. Lett. **25**, 807 (1970).
- [35] F. Amet, J. R. Williams, K. Watanabe, T. Taniguchi, and D. Goldhaber-Gordon, Phys. Rev. Lett. **110**, 216601 (2013).